PRAMANA
— journal of
physics

Vol. 67, No. 6
December 2006
pp. 1141–1154

Vapour–liquid equilibria of the two- and three-dimensional monoatomic classical fluids interacting via double Yukawa potential

Y PATHANIA and P K AHLUWALIA
Physics Department, Himachal Pradesh University, Shimla 171 005, India
E-mail: yogyatapathania@yahoo.com

MS received 30 November 2005; revised 31 May 2006; accepted 11 September 2006

Abstract. We have carried out Monte Carlo simulations in Gibbs ensemble for two- and three-dimensional double Yukawa fluid. We have compared liquid–vapour equilibrium curve with that of Lennard-Jones, when parameters occurring in double Yukawa potential are chosen to fit Lennard-Jones potential. The results are in good agreement. The role of repulsive and attractive contributions for the potential on the liquid–vapour coexistence region as well as on critical temperature and critical density has been studied. The critical temperature is found to be more sensitive than the critical density to the variation in repulsive and attractive parts of the potential. Also, the range of the attractive interaction directly influences range of the liquid–vapour coexistence region. It has been found that smaller the values of the attractive parameter, larger is the coexistence region.

Keywords. Monte Carlo simulations; Gibbs ensemble; monoatomic classical fluids; double Yukawa potential.

PACS Nos 02.70.Uu; 68.03.-g; 68.18.Jk

1. Introduction

Phase transitions of real and model complex fluids are of significant scientific and technological interest. From a modeling point of view, it is often of considerable interest to predict, as accurately as possible, the phase behaviour of a simplified system containing the essential interactions of interest. Computer simulations are a natural choice for this purpose, as they allow complete freedom in the specification of the model potential. However, prediction of the order and the precise location of phase transitions from simulations is not a simple matter. Phase transitions are collective phenomena that are not directly accessible by molecular dynamics or simple constant volume Monte Carlo simulations. Many specialised techniques have been developed [1–5] to study the phase transitions.

Here, we focus on a relatively simple and computationally inexpensive set of techniques known collectively as 'Gibbs ensemble' method [1]. While the Gibbs ensemble does not necessarily provide data of the highest possible accuracy and

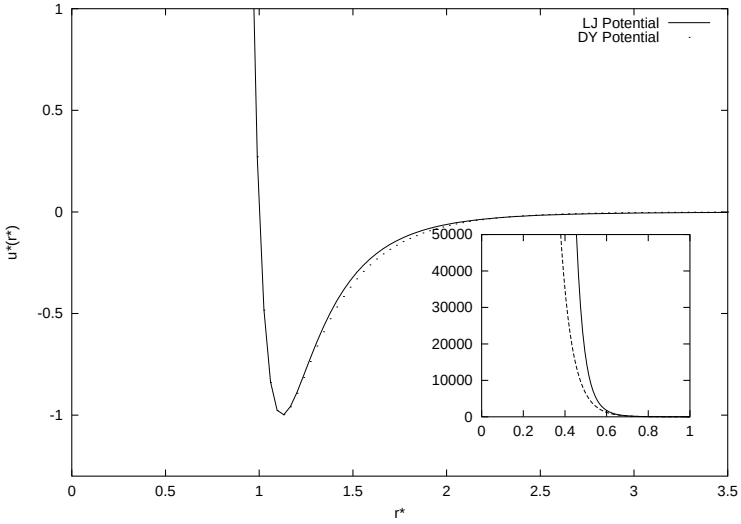

Figure 1. The double Yukawa potential with parameters $\lambda_1 = 14.735$, $\lambda_2 = 2.6793$ and $E = 2.0198\epsilon$ showing a close fit to Lennard-Jones potential. Inset shows that the repulsive potential energy for DY potential is less when compared to LJ potential as r^* decreases.

is not applicable to many important classes of systems, it is most commonly used for obtaining the phase behaviour of fluids and mixtures. The reason for this widespread use is probably the simplicity of the method having an intuitive physical basis, easy description and programming. It requires minimal information from the user regarding the approximate location of phase diagram or other aspects of the behaviour of a new system under study.

The full phase behaviour of hard spheres has been computed with short-range attractive Yukawa interaction using MC computer simulation techniques [6] and with repulsive Yukawa interactions for charged colloids [7]. In this paper, we present the application of the Gibbs ensemble technique to obtain the vapour–liquid curve, respectively, of the two- and three-dimensional monoatomic fluids interacting via double Yukawa potential, when parameters are chosen to fit LJ potential. These are followed by the study of the role of attractive and repulsive potentials on liquid–vapour transition as well as on the coexistence region. The double Yukawa potential has been discussed in detail in §2. The main motivation behind using this potential is that it can be fitted to any realistic potential to facilitate the calculations of the thermodynamic properties of classical fluids [8–10]. This potential has also been used to deal with long-range correlations [11]. If suitably parameterised, DY potential provides a close fit to LJ potential as shown in figure 1. Though both the potentials agree well if we look at the attractive bowl of the potential, on looking at the repulsive part in the range $0 < r^* < 1$, it has been found that as the value of r^* decreases, magnitude of repulsive potential energy for DY potential goes on decreasing as compared to the magnitude of LJ potential, which is shown in the inset of figure 1. Thus DY potential is convenient to use due to soft repulsion when compared to LJ potential [12].

The simulation details of the MC method are given in §3. Section 4 discusses the role of attractive and repulsive potentials on liquid–vapour transition as well as on the coexistence region. Concluding remarks are given in §5.

2. Double Yukawa potential

The form of this potential is

$$u(r) = E\epsilon \left(\frac{\sigma}{r}\right) \left\{ \exp\left(-\lambda_1 \left(\frac{r}{\sigma} - 1\right)\right) - \exp\left(-\lambda_2 \left(\frac{r}{\sigma} - 1\right)\right)\right\}, \tag{1}$$

where σ is the value of r at which $u(r) = 0$, E is the depth of the potential and ϵ is an arbitrary energy scale. λ_1 and λ_2 control the decay range of the repulsive and attractive contributions to the potential.

The nature of the potentials for different λ_1 and λ_2 are shown in figures 2 and 3, respectively. λ_1 affects considerably the repulsive and, to a lesser extent, the attractive parts of the potential. On the other hand, λ_2 affects mainly the attractive part of the potential. The impact of λ_2 on the range of attractive part can be clearly seen. The locations and depths of the minima of the attractive potentials, however are strongly dependent on both λ_1 and λ_2. We can calculate the locations, $r^*_{\min}$, of the minima from

$$r^*_{\min} = 1 + \frac{1}{(\lambda_1 - \lambda_2)} \log\left(\frac{\lambda_1 r^*_{\min} + 1}{\lambda_2 r^*_{\min} + 1}\right). \tag{2}$$

For a given λ_2, $r^*_{\min}$ decreases whereas $|u_{\min}|$ increases with increasing λ_1. Similarly, $r^*_{\min}$ also decreases with increasing λ_2 but $|u_{\min}|$ decreases considerably.

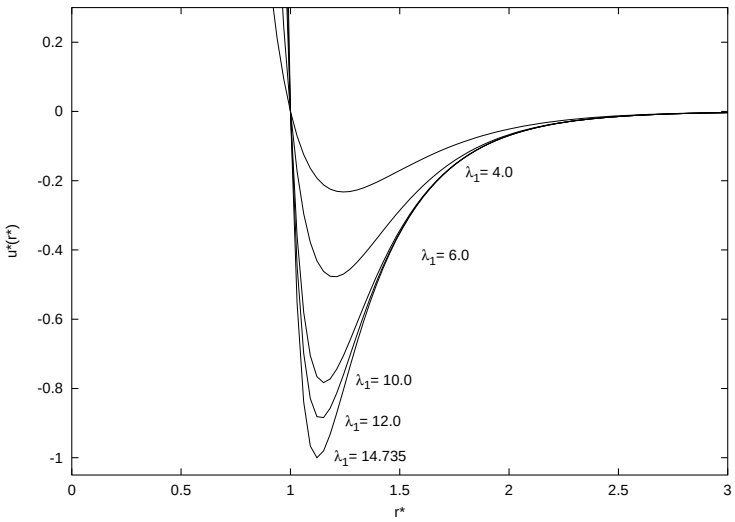

Figure 2. The double Yukawa potential for different values of λ_1, with $\lambda_2 = 2.6793$.

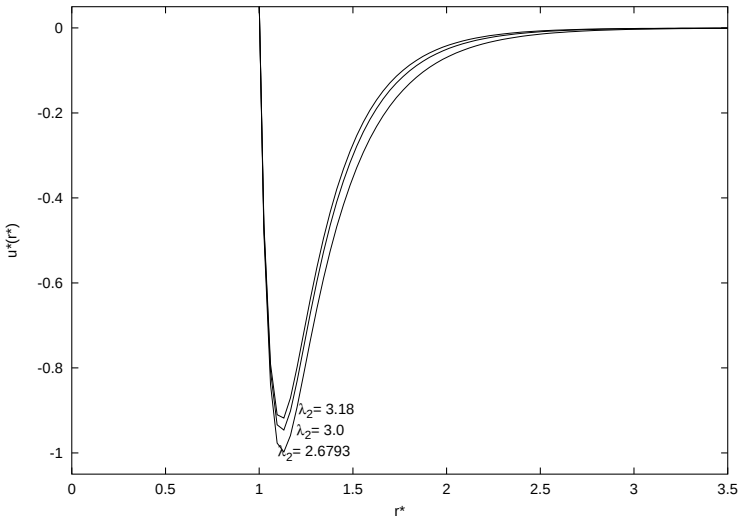

Figure 3. The double Yukawa potential for different values of λ_2, with $\lambda_1 = 14.735$.

3. Computational implementation

We have chosen to start our simulation with 256 particles on a simple cubic lattice for 3D fluids and on a square lattice for 2D fluids. In both 2D and 3D fluids MC calculations were performed for the two systems each interacting with LJ and DY potentials, respectively. In each system, the particles were distributed over two volumes, i.e. Box1 and Box2. The simulation was started with equal density, ρ, in both boxes. The potential was truncated at approximately half the box length and then shifted. A correction was made to take into account the effect of the neglected tail on the thermodynamic quantities. Periodic boundary conditions were imposed in the usual fashion. With the periodic boundary conditions, we eliminated the surfaces and created a quasi-infinite volume/area to represent the macroscopic system more closely. Thermodynamic requirements for phase coexistence are that each region should be in internal equilibrium, and that temperature, pressure and chemical potentials of all components should be the same in the two regions. Only the system temperature in Monte Carlo simulations is specified in advance. The remaining three conditions, i.e. internal equilibrium, equality of pressure and equality of chemical potential, are respectively satisfied by performing three types of Monte Carlo 'moves', viz., displacements of particles within each region (to satisfy internal equilibrium), fluctuations in the volume of the two regions (to satisfy equality of pressures) and transfers of particles between regions (to satisfy equality of chemical potentials of all components).

The acceptance rules for these steps in the Gibbs ensemble can be derived from the condition of detailed balance

$$K(\mathrm{o} \to \mathrm{n}) = k(\mathrm{n} \to \mathrm{o}), \tag{3}$$

where $K(\mathrm{o} \to \mathrm{n})$ is the flow of configuration, from old configuration to new configuration, i.e. $\mathrm{o} \to \mathrm{n}$, which is equal to the product of the probability of being in configuration o (old), $N(\mathrm{o})$, the probability of generating configuration n (new), $\alpha(\mathrm{o} \to \mathrm{n})$; and the probability of accepting this move, $\mathrm{acc}(\mathrm{o} \to \mathrm{n})$, i.e.

$$K(\mathrm{o} \to \mathrm{n}) = N(\mathrm{o}) \times \alpha(\mathrm{o} \to \mathrm{n}) \times \mathrm{acc}(\mathrm{o} \to \mathrm{n}). \tag{4}$$

For a displacement step, the probability of accepting the move is given by

$$\mathrm{acc}(\mathrm{o} \to \mathrm{n}) = \min(1, \exp\{-\beta[U(s_{\mathrm{n}}^{n_1}) - U(s_{\mathrm{o}}^{n_1})]\}), \tag{5}$$

where $\beta = 1/K_{\mathrm{B}}T$, s_{o} and s_{n} are the scaled coordinates of the particles in the old and new configurations, respectively and $U(s_{\mathrm{o}}^{n_1})$ and $U(s_{\mathrm{n}}^{n_1})$ are the total intermolecular potentials of interaction of n_1 particles in the old and new configurations, respectively.

For a volume change step, the probability of acceptance is given by

$$\mathrm{acc}(\mathrm{o} \to \mathrm{n}) = \min\left\{1, \left(\frac{V_1^{\mathrm{n}}}{V_1^{\mathrm{o}}}\right)^{n_1+1} \left(\frac{V - V_1^{\mathrm{n}}}{V - V_1^{\mathrm{o}}}\right)^{N-n_1+1} \times \exp\left\{-\beta[U(s_{\mathrm{n}}^N) - U(s_{\mathrm{o}}^N)]\right\}\right\}. \tag{6}$$

The acceptance criterion for particle transfer is

$$\mathrm{acc}(\mathrm{o} \to \mathrm{n}) = \min\left\{1, \frac{n_1(V - V_1)}{(N - n_1 + 1)V_1} \exp\left\{-\beta\left[U(s_{\mathrm{n}}^N) - U(s_{\mathrm{o}}^N)\right]\right\}\right\}. \tag{7}$$

The conditions between the pressure P and chemical potential μ satisfied by these two sets of moves (i.e. particle transfer and volume exchange) are then

$$\begin{aligned} P_{\mathrm{L}}(\rho_{\mathrm{L}}, T) &= P_{\mathrm{V}}(\rho_{\mathrm{V}}, T), \\ \mu_{\mathrm{L}}(\rho_{\mathrm{L}}, T) &= \mu_{\mathrm{V}}(\rho_{\mathrm{V}}, T), \end{aligned} \tag{8}$$

where subscripts L and V represent the liquid and vapour phases, respectively. The chemical potential can be obtained from

$$u_1 = -k_{\mathrm{B}}T \ln \frac{1}{\Lambda^3} \left\langle \frac{V_1}{n_1 + 1} \exp(-\beta \Delta U_1^+) \right\rangle_{\text{Gibbs, Box1}}, \tag{9}$$

where Λ is the thermal de Broglie wavelength, ΔU_1^+ is the energy of a (ghost) particle in Box1 and $\langle \cdots \rangle_{\text{Gibbs, Box1}}$ denotes an ensemble average in the Gibbs ensemble restricted to Box1. This ensemble average is valid only if the boxes do not change identity during a simulation.

After an equilibration of 10,000 Monte Carlo cycles, a further 30,000 cycles were used to accumulate the averages of various thermodynamic properties. Each cycle was composed of 200 attempted displacements, 2 volume fluctuations and 20 particle interchanges.

The simulations have also been carried out for 512 and 1024 particles to study the finite size effects. However, the result comes out to be approximately same as that for 256 particles.

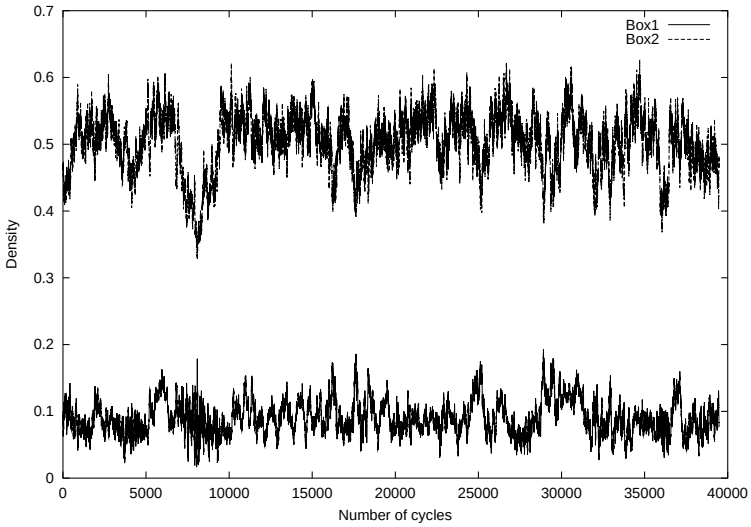

Figure 4. Reduced density of the two boxes of the Gibbs ensemble as a function of the number of Monte Carlo cycles for a system of 3D double Yukawa fluid. The number of particles was $N = 256$ and temperature $T^* = 1.2$.

4. Results and discussion

Approaching critical points by simulations is complicated by the use of a finite system and periodic boundary conditions. When the 2D and 3D systems are away from their respective critical point of the phase transition as shown in figures 4 and 6, one box evolves into a liquid density and the other to a gas density. The equilibrium densities and compositions of each coexisting phase can be simply determined by averaging the observations after equilibration. As one approaches a critical point even closer, the probability of formation of interfaces is small, and there are frequent exchanges of the identity of two boxes as shown in figures 5 and 7.

The liquid–vapour coexistence curves for two- and three-dimensional monoatomic fluids interacting via truncated and shifted DY potential are shown in figures 8 and 9, respectively. Here, the parameters of DY potential are chosen to fit LJ potential. It is evident that both the curves yield closer agreement. The curves calculated for different λ_1 and λ_2 are plotted in figures 10, 11 and 12, 13 for 2D and 3D fluids respectively. From these figures, we find that our values failed to converge to a precise critical point. This is also the case for recent computer simulation results [13,14].

To estimate the critical point we have fitted our results to the law of rectilinear diameters [15]

$$\frac{\rho_{\mathrm{l}} + \rho_{\mathrm{g}}}{2} = \rho_{\mathrm{c}} + A(T - T_{\mathrm{c}})$$

and the scaling law for the density [16]

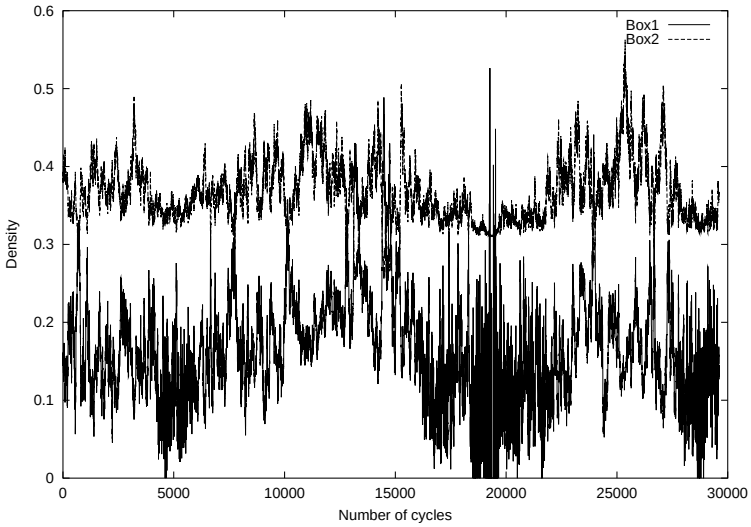

Figure 5. Reduced density in the two boxes in a Gibbs ensemble simulation close to the critical temperature in 3D DY fluid.

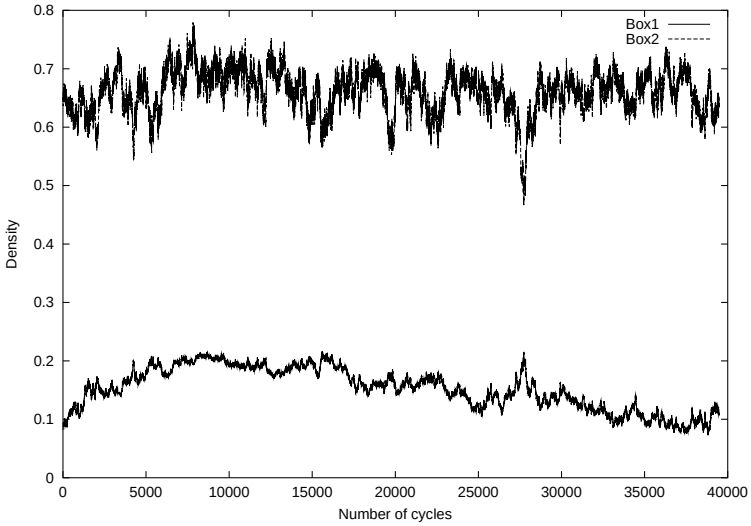

Figure 6. Reduced density of the two boxes of the Gibbs ensemble as a function of the number of Monte Carlo cycles for a system of 2D double Yukawa fluid. The number of particles was $N = 256$ and temperature $T^* = 0.50$.

$$\rho_{\mathrm{l}} - \rho_{\mathrm{g}} = B(T - T_{\mathrm{c}})^{\beta},$$

where $\rho_{\mathrm{l}}(\rho_{\mathrm{g}})$ is the density of the liquid(gas) phase, ρ_{c} the critical density and T_{c} the critical temperature. β is the critical exponent. For three-dimensional systems $\beta = 0.32$ and for two-dimensional systems $\beta = 0.125$ [16]. A and B depend on the system and are obtained from the fit.

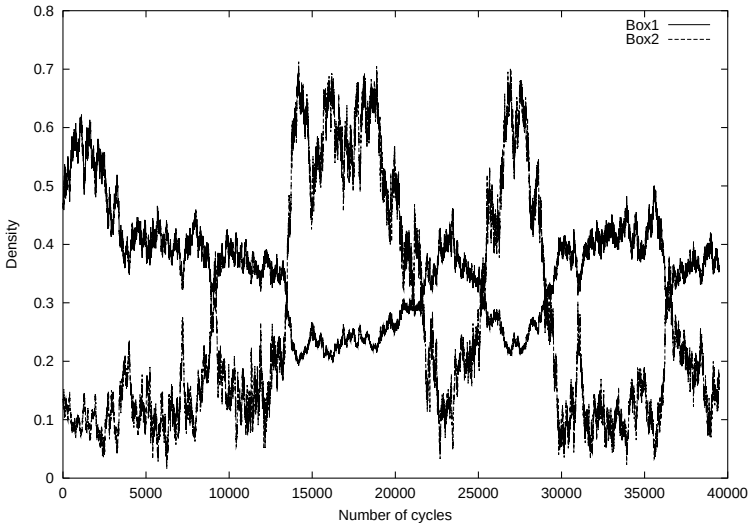

Figure 7. Reduced density in the two boxes in a Gibbs ensemble simulation close to the critical temperature in 2D DY fluid.

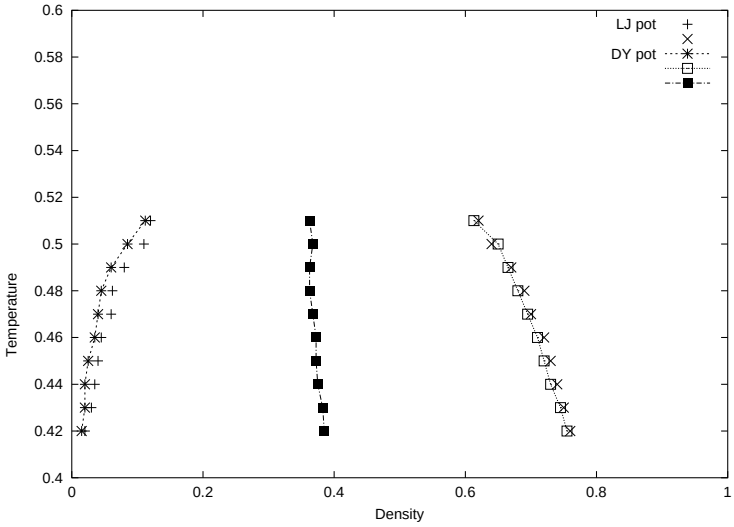

Figure 8. Phase diagram of 2D double Yukawa fluid denoted by linepoints. Points denote the phase diagram of Lennard–Jones fluid.

The results for the critical points at different steepness parameters λ_1 and λ_2 are listed in tables 1 and 2 for 2D and 3D fluids, respectively. The 3D results are compared with the statistical mechanical based theory results of Ali *et al* [11]. Our values for critical temperature and critical density are found to be lower when compared to that of Ali *et al* [11]. These discrepancies may be due to approximations that go into the statistical mechanical calculations.

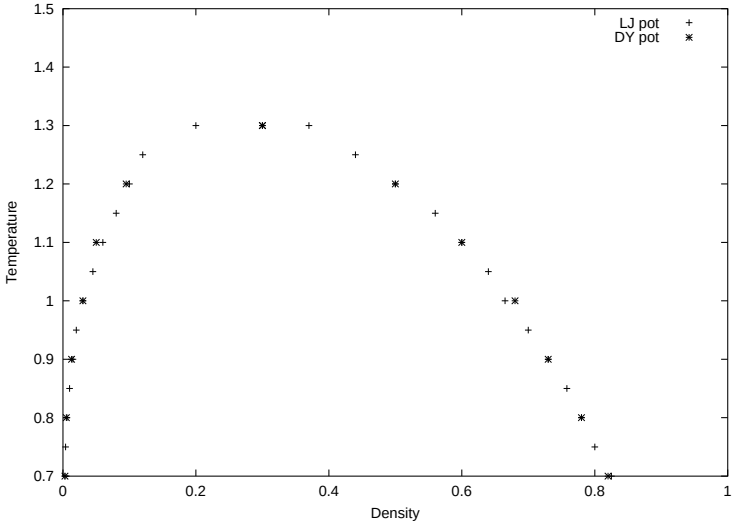

Figure 9. Phase diagram of 3D double Yukawa fluid. The curve shows good agreement with the phase diagram of Lennard–Jones fluid.

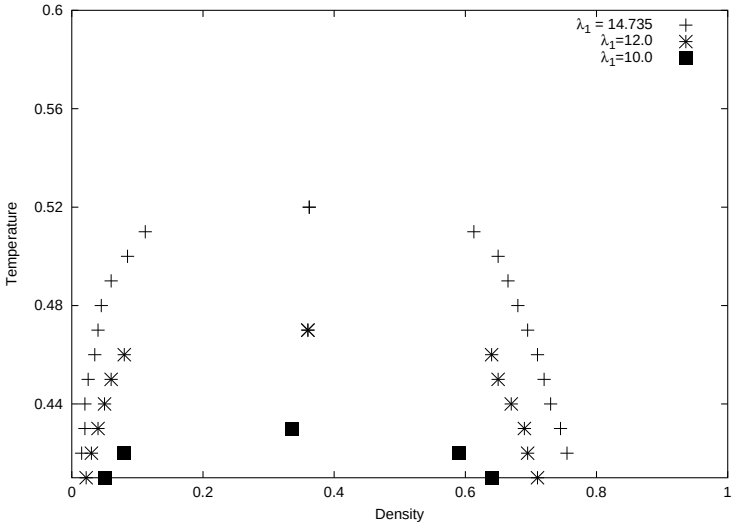

Figure 10. Phase diagram of 2D double Yukawa fluid when λ_1 is varied.

However, when the parameters of DY potential are chosen to fit LJ potential, the value of critical temperature and critical density are found to agree well with the results obtained by simulation, when particles interact via LJ potential. For the 3D truncated and shifted Lennard-Jones fluid, Smit [17] has obtained the estimate for critical point to be $T_c^* = 1.316 \pm 0.006$ and $\rho_c^* = 0.304 \pm 0.006$ via Gibbs ensemble simulations, which in our case is $T_c^* = 1.315 \pm 0.0021$ and $\rho_c^* = 0.3013 \pm 0.0020$. He has also shown that the truncation of the potential has a large effect on the phase

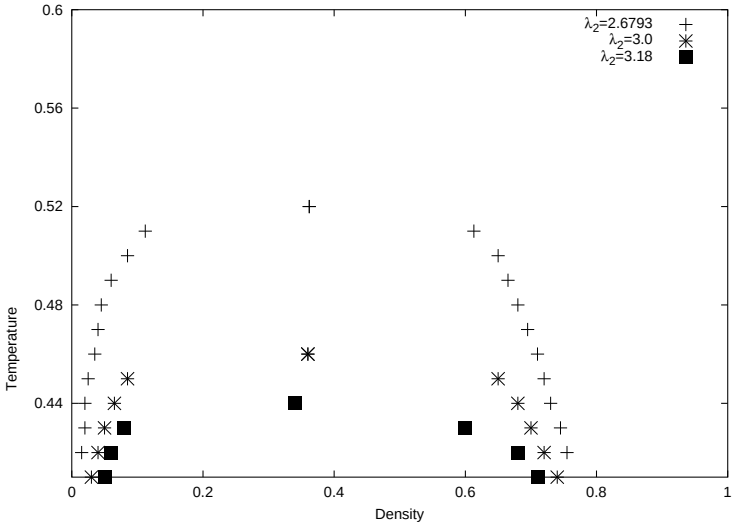

Figure 11. Phase diagram of 2D double Yukawa fluid when λ_2 is varied.

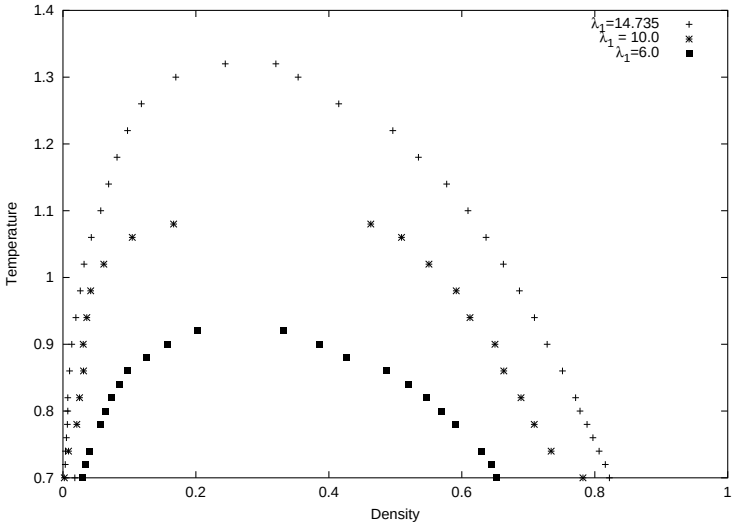

Figure 12. Phase diagram of 3D double Yukawa fluid when λ_1 is varied.

behaviour. Lotfi *et al* [2] used a combination of NPT simulations and particle insertion to determine the coexistence curve for 3D LJ fluid. The estimate of the critical point obtained by them is $T_c^* = 1.310$ and $\rho_c^* = 0.314$.

Smit and Frenkel [18] also obtained the estimate for critical point for 2D truncated and shifted potential via Gibbs ensemble simulation technique to be $T_c^* = 0.515 \pm 0.002$ and $\rho_c^* = 0.355 \pm 0.003$, which in our case comes out to be $T_c^* = 0.5151 \pm 0.0041$ and $\rho_c^* = 0.3587 \pm 0.0021$. The values are in good agreement.

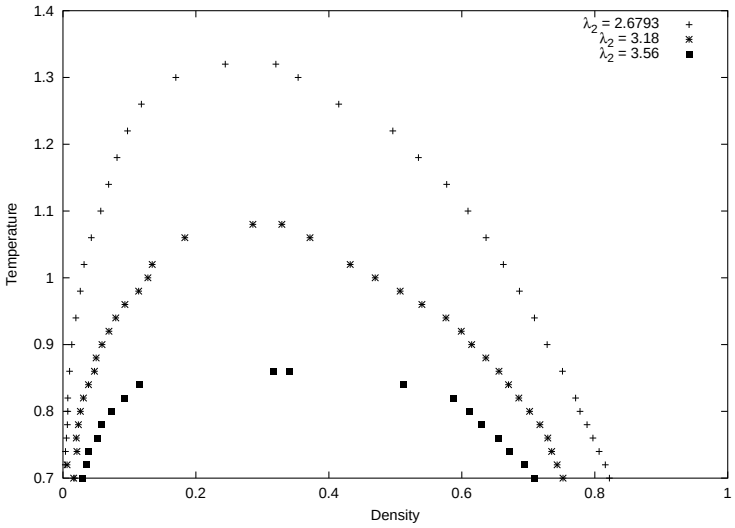

Figure 13. Phase diagram of 3D double Yukawa fluid when λ_2 is varied.

The critical temperature is found to be more sensitive than the critical density to the variation in λ_1 and λ_2, and, in turn, on the depths of the attractive potential. Larger the value of repulsive core (λ_1), higher is the value of T_c as shown in figures 10 and 12. Also, the range of the attractive interaction directly influences the range of the liquid–vapour coexistence region. Smaller the values of λ_2, larger is the coexistence region as shown in figures 11 and 13.

The liquid–vapour coexistence region is measured approximately by the ratio T_c/T_{tr}, where T_{tr} represents the triple point temperature, and varies between different classes of substance, i.e., on the analytic form of the intermolecular potential. It is only the depth of the potential well that determines the coexistence region. With the decrease in the repulsive core of the DY potential, i.e. λ_1, the depth of the potential well decreases (figure 2) and hence the liquid–vapour coexistence region decreases and vice versa as shown in figures 10 and 12. Also on increasing the attractive parameter λ_2 of DY potential, depth of potential well decreases (figure 3) and hence the liquid–vapour coexistence region as shown in figures 11 and 13.

Table 1. Critical point properties for 2D DY fluid at different steepness parameters λ_1 and λ_2.

λ_1	λ_2	ρ_c^*	T_c^*
14.735	2.6793	0.3587	0.5151
	3.0	0.3653	0.4550
	3.18	0.3333	0.4351
14.735	2.6793	0.3587	0.5151
12.0		0.3564	0.4650
10.0		0.3300	0.4250

Table 2. Comparison of critical point properties for 3D DY fluid at different steepness parameters λ_1 and λ_2 with the statistical mechanical based theory of Ali *et al* [11].

		Present work		Results of Ali *et al* [11]	
λ_1	λ_2	ρ_c^*	T_c^*	ρ_c^*	T_c^*
14.735	2.6793	0.2732	1.315	0.3013	1.4459
	3.18	0.2837	1.085	0.3002	1.1725
	3.56	0.3201	0.865	0.3144	1.0156
14.735	2.6793	0.2732	1.315	0.3013	1.4459
10.0		0.2866	1.125	0.2923	1.2748
6.0		0.2675	0.925	0.2915	0.9836

Table 3. Comparison of pressure (P^*), chemical potential (μ^*) and liquid–vapour densities (ρ_L^* and ρ_V^*) expressed in reduced units along the liquid–vapour coexistence curve in both boxes for 2D DY fluid.

	Liquid side			Vapour side		
T^*	ρ_L^*	P^*	μ^*	ρ_V^*	P^*	μ^*
0.42	0.755	0.007	−1.853	0.015	0.008	−1.885
0.43	0.745	0.009	−1.824	0.020	0.011	−1.847
0.44	0.730	0.011	−1.790	0.020	0.010	−1.739
0.45	0.720	0.010	−1.815	0.025	0.009	−1.829
0.46	0.710	0.014	−1.793	0.035	0.016	−1.752
0.47	0.695	0.012	−1.760	0.040	0.013	−1.762
0.48	0.680	0.017	−1.736	0.045	0.018	−1.755
0.49	0.665	0.018	−1.739	0.060	0.021	−1.750
0.50	0.650	0.026	−1.715	0.100	0.027	−1.672
0.51	0.600	0.026	−1.729	0.150	0.025	−1.709

The liquid–vapour coexistence envelope for 2D fluids is found to be over considerably narrower temperature range when compared to its 3D counterpart (figures 8 and 9). This may be due to the effect of dimensionality.

Our calculations for both 2D and 3D fluids show that the values of P^* and μ^* are equal for both sides of the coexistence curve under equilibrium conditions as shown in tables 3 and 4.

5. Conclusions

Gibbs ensemble simulation method has been applied to investigate the liquid–vapour equilibrium of monoatomic fluids interacting with DY potential, which encounters a transition from a short-range ordered to the disordered phase. The

Table 4. Comparison of pressure (P^*), chemical potential (μ^*) and liquid–vapour densities (ρ_L^* and ρ_V^*) expressed in reduced units along the liquid–vapour coexistence curve in both boxes for 3D DY fluid.

	Liquid side			Vapour side		
T^*	ρ_L^*	P^*	μ^*	ρ_V^*	P^*	μ^*
0.70	0.8220	0.0048	−5.100	0.0178	0.0052	−3.937
0.74	0.8065	0.0026	−4.057	0.0038	0.0027	−4.787
0.78	0.7884	0.0048	−4.357	0.0066	0.0049	−4.076
0.82	0.7711	0.0050	−4.160	0.0072	0.0054	−4.157
0.86	0.7515	0.0074	−3.884	0.0099	0.0078	−4.094
0.90	0.7283	0.0092	−4.008	0.0133	0.0110	−3.983
0.94	0.7092	0.0150	−3.917	0.0195	0.0162	−3.916
0.98	0.6867	0.0210	−3.864	0.0261	0.0219	−3.872
1.02	0.6625	0.0269	−3.838	0.0318	0.0271	−3.802
1.06	0.6365	0.0354	−3.764	0.0427	0.0356	−3.773
1.10	0.6093	0.0460	−3.735	0.0568	0.0464	−3.738
1.14	0.5772	0.0559	−3.694	0.0687	0.0558	−3.689
1.18	0.5347	0.0654	−3.698	0.0813	0.0656	−3.678
1.22	0.4862	0.0344	−3.643	0.1072	0.0345	−3.639
1.26	0.3749	0.0662	−3.650	0.1179	0.0663	−3.577
1.30	0.3538	0.1098	−3.550	0.1697	0.1136	−3.576

calculations have been first carried out in two dimensions and then extended to three dimensions. Some of the important results of the present work are as follows:

(a) The DY potential has paved the way to analyse the role of attractive and repulsive potentials on liquid–vapour transition as well as on the coexistence region. The critical temperature (T_c^*) is found to be more sensitive than the critical density to the depth of the attractive potential. Larger the attractive depth, higher is the value of T_c^* which is in close agreement with the statistical mechanical based theory of Ali *et al* [11].

(b) The values of critical temperature T_c^* and critical density ρ_c^* are found to be lower when compared to those calculated by Ali *et al* [11], which may be due to the approximation that go into the statistical mechanical calculations. When parameters occurring in DY potential are chosen to fit LJ potential, T_c^* and ρ_c^* agree well with the results obtained by simulation, when the particles interact via LJ potential.

(c) The range of the attractive interaction (through λ_2) directly influences the range of the L–V coexistence region. Smaller the values of λ_2, larger is the coexistence region. Also, the range of L–V equilibrium temperature shrinks as the range of attractive interaction of DY fluid decreases, which matches with the results of Shukla [19].

(d) The liquid–vapour coexistence envelope for 2D fluids is found to be over considerably narrower temperature range when compared to its 3D counterpart. This may be because of dimensionality.

References

[1] A Z Panagiotopoulos, *Mol. Phys.* **61**, 813 (1987)
[2] A Lotfi, J Vrabec and J Fischer, *Mol. Phys.* **76**, 1319 (1992)
[3] G M Torrie and J P Valleau, *J. Comp. Phys.* **23**, 187 (1977)
[4] J P Valleau, *J. Comp. Phys.* **96**, 193 (1991)
[5] A Z Panagiotopoulos, *Mol. Sim.* **9**, 1 (1992)
[6] M Dijkstra, *Phys. Rev.* **E66**, 021402 (2002)
[7] A P Hynninen and M Dikkstra, *J. Phys.: Condens. Matter* **15**, S3557 (2003)
[8] S M Foiles and N W Aschcroft, *J. Chem. Phys.* **75**, 3594 (1981)
[9] D J Gonzalez and M Silbert, *J. Phys.* **C16**, 1097 (1983)
[10] A Garcia and D J Gonzalez, *Phys. Chem. Liq.* **18**, 91 (1988)
[11] I Ali, S M Osman, M Al-Busaidi and R N Singh, *Int. J. Mod. Phys.* **B13(27)**, 3261 (1999)
[12] Y Pathania and P K Ahluwalia, *Pramana – J. Phys.* **65(3)**, 457 (2005)
[13] E Lomba and N G Almarza, *J. Chem. Phys.* **100**, 8367 (1994)
[14] L Mederos and G Navascues, *J. Chem. Phys.* **101**, 8841 (1994)
[15] J S Rowlinson and F L Swinton, *Liquids and liquid mixtures*, 3rd edn. (Butterworth, London, 1982)
[16] J S Rowlinson and B Widom, *Molecular theory of capillarity* (Clarendon Press, Oxford, 1982)
[17] B Smit, *J. Chem. Phys.* **96(11)**, 8639 (1992)
[18] B Smit and D Frenkel, *J. Chem. Phys.* **94(8)**, 5663 (1991)
[19] K P Shukla, *J. Chem. Phys.* **112(23)**, 10358 (2000)